*Desalination and Water Treatment*
www.deswater.com

doi: 10.5004/dwt.2021.27647

234 (2021) 288–298
September

# A cross-linked chitosan-Schiff base: new material for the removal of methyl orange from aqueous solution

Furqan Mohammed Hussein[a], Hamida Edan Salman[a], Asim A. Balakit[b,*]

[a]*Chemistry Department, College of Education for Pure Sciences, University of Kerbala, Iraq, emails: fo33.rqn@gmail.com. (F.M. Hussein), hamida.idan@uokerbala.edu.iq (H.E. Salman)*
[b]*College of Pharmacy, University of Babylon, Babylon, Iraq, email: asim_alsalehi@hotmail.com*

Received 10 March 2021; Accepted 24 July 2021

**ABSTRACT**

A cross-linked chitosan-Schiff base (denoted as CCSB) was synthesized by the condensation of salicylaldehyde with chitosan followed by cross-linking with glutaraldehyde, the synthesized polymer was characterized by Fourier-transform infrared spectroscopy, scanning electron microscopy, and energy-dispersive X-ray spectroscopy techniques. The new polymer was tested as an adsorbent to remove the organic dye methyl orange (MO) from aqueous solutions. The effects of contact time (1–180 min), pH (2–10), and initial dye concentration (200–500 ppm) were studied. The experimental equilibrium data for the adsorption process were fitted to Langmuir, Freundlich, and Temkin isotherm models, the best fit was with Langmuir isotherm model, the correlation coefficient ($R^2$) value for this isotherm was (0.9984), while for Freundlich, and Temkin isotherms the $R^2$ values were 0.8631 and 0.9212 respectively. The experimental adsorption capacity values were found to be 99.01–233.8 mg/g, and the dye removal percentage values were 93.52%–99.01%. The results of the kinetic studies revealed that the adsorption of MO on CCSB is a pseudo-second-order process, with $R^2$ value of 1, and the calculated adsorption capacity ($q_e$) values for this model are very close to the obtained experimental results. The thermodynamic parameters indicated that the adsorption happens spontaneously as negative $\Delta G$ values were obtained, endothermic process with positive $\Delta H$ (9.317 kJ/mol) and positive $\Delta S$ (71.018 J/mol/K) which means that the disorder of molecules increases at the adsorbent-solution interface.

*Keywords:* Water treatment; Adsorption; Methyl orange; Chitosan; Schiff base

## 1. Introduction

Contamination of water with organic pollutants discharged by industries causes a negative impact on the aquatic ecosystem [1]. Organic dyes are used in a broad spectrum of industrial processes since they are used as coloring agents for textiles, cosmetics, and plastics [2]. The textile dyes are considered mutagenic, carcinogenic, and toxic agents [3]. Accordingly, the removal of such hazardous materials from wastewater by water treatment processes has become an interesting issue. Researchers have developed different strategies for wastewater treatment, the reported methodologies are based on the concepts of adsorption, reverse osmosis, ultrafiltration, oxidation, and ozonation [4–6]. The relative simplicity of implementation and cost-effectiveness of using adsorbents in water treatment technologies make adsorption is the favored and widely used method [7].

Various materials have been developed and investigated as organic dye adsorbents including active carbon [8], synthetic polymers [9], natural polymers [10], and biological biomasses [11]. To enhance the efficiency of the adsorbents in dye removal processes, different structural modifications have been reported, such modifications aimed to increase

* Corresponding author.

the surface area of the adsorbent as they affect the surface morphology, and provide it with a variety of pendant groups that interact with the target dyes and hence increase the adsorption capacity and improve the performance of the used materials [12–14]. Biopolymers are the materials of choice for different applications because they are eco-friendly, available, and have good mechanical properties [15–17].

Chitosan is a natural biopolymer with distinctive properties such as biocompatibility, biodegradability, and non-toxicity; accordingly, it has been reported as starting material in the development of new polymers for water treatment purposes [18]. The availability of free $-NH_2$ groups in the structure of chitosan makes it liable for modification by reacting it with different organic molecules such as aldehydes that undergo a condensation reaction with the amino groups giving polymeric Schiff bases. In a recent study, a chitosan-Schiff base with heterocyclic moieties has been introduced as an adsorbent to remove methyl orange from aqueous solutions, the heterocyclic aldehyde was synthesized by three steps, then it was used to modify the chitosan [19]. To develop a new adsorbent based on chitosan modification with a readily available aldehyde, in short, energy-saving and cost-efficient synthetic pathway, here we introduce a cross-linked chitosan-Schiff base synthesized by the reaction of chitosan with salicylaldehyde followed by cross-linking with glutaraldehyde, and we have tested this material as adsorbent to remove methyl orange from aqueous solutions.

## 2. Materials and methods

Chitosan (molecular formula: $(C_6H_{11}NO_4)_n$; degree of deacetylation: 75%; molecular weight: 3,800–20,000 Daltons) was obtained from HiMedia. All of the other used chemicals were obtained from commercial sources and used as received.

### 2.1. Methods

#### 2.1.1. Synthesis of cross-linked chitosan-Schiff base

The cross-linked chitosan-Schiff base (CCSB) was synthesized according to a reported protocol with some modifications [20]. Chitosan (1.30 g) was dissolved in acetic acid (1%, 100 mL), solution of salicylaldehyde (1.0 mL) in ethanol (10 mL) was added slowly to the chitosan solution followed by stirring for 6 h at room temperature to get the chitosan-Schiff base (CSB). Glutaraldehyde (25.0%, 5.0 mL) was added in a dropwise manner with continuous stirring for 30 min. The product (CSB) was collected by filtration, washed thoroughly with acetone, and dried, Fig. 1 shows the synthesis steps.

### 2.2. Characterization

#### 2.2.1. Fourier-transform infrared spectroscopy

The Fourier-transform infrared (FT-IR) spectra of the chitosan, chitosan-Schiff base (CSB), and CCSB were recorded on FT-IR spectrophotometer (Tensor II, Bruker, Germany) and by KBr disc technique.

#### 2.2.2. Scanning electron microscopy and energy-dispersive X-ray spectroscopy analysis

Scanning electron microscopy (SEM) and energy-dispersive X-ray spectroscopy (EDS) analysis were recorded on Quanta 450 FEI scanning electron microscope (voltage 30 kV, spot size 3 mm and magnification range 8,565–10,316 X with 5.0 μm scale bar) equipped with XFlash® 6-10 detector.

### 2.3. Adsorption studies

The adsorption experiments were conducted by shaking suspensions of a fixed weight of CCS (0.1 g) in 50.0 mL of different concentrations of aqueous methyl orange (MO) solution, 5 mL portions were withdrawn, filtered and the absorbance was measured at 464 nm using the UV-Vis spectrophotometer (Shimadzu-1800, Japan) to determine the dye concentration. The adsorption capacity of CCSB ($q_e$, amount of MO adsorbed in mg/weight of CCS in g) was determined according to Eq. (1) [21]:

$$q_e = \frac{\left(C_0 - C_e\right)V}{W} \tag{1}$$

where $C_0$ and $C_e$ are the initial and equilibrium MO concentration (mg/L), respectively, $V$ is the volume of MO solution (L) and $W$ is the weight of CCSB (g). The time required for equilibrium was determined by running experiments at different time intervals, the time of the other experiments was set accordingly. The pH was adjusted by using 0.1 M solutions of HCl and NaOH. The thermodynamic parameters were studied by running adsorption experiments at different temperatures (298, 303, 308, and 313 K).

## 3. Results and discussion

### 3.1. Synthesis and characterization of CCSB

The CCSB has been synthesized via one-pot two steps synthesis, the first step involves the formation of the chitosan-Schiff base (CSB) by the condensation of salicylaldehyde with chitosan [20]. The resulted polymer was then cross-linked by its treatment with glutaraldehyde.

*Scheme 1. Synthesis of CCSB*

To confirm the formation of the chitosan-Schiff base (CSB), a test experiment was performed without adding the cross-linker (glutaraldehyde), the product was precipitated by acetone and dried. The FT-IR spectrum was recorded for the product, Fig. 2 shows the FT-IR spectra of chitosan, CSB, and CCSB. The appearance of characteristic absorption at 1,629.9 $cm^{-1}$ indicates the formation of C=N by the condensation of salicylaldehyde with chitosan to form the Schiff base, furthermore, the bands at 1,498.7 and 1,460.1 $cm^{-1}$ correspond to the phenyl ring were also observed in the spectrum which confirms the formation of CSB. The main characteristic absorption band can be observed in the spectrum of the CCSB is 1,645.3 $cm^{-1}$ which is corresponding to the C=N.

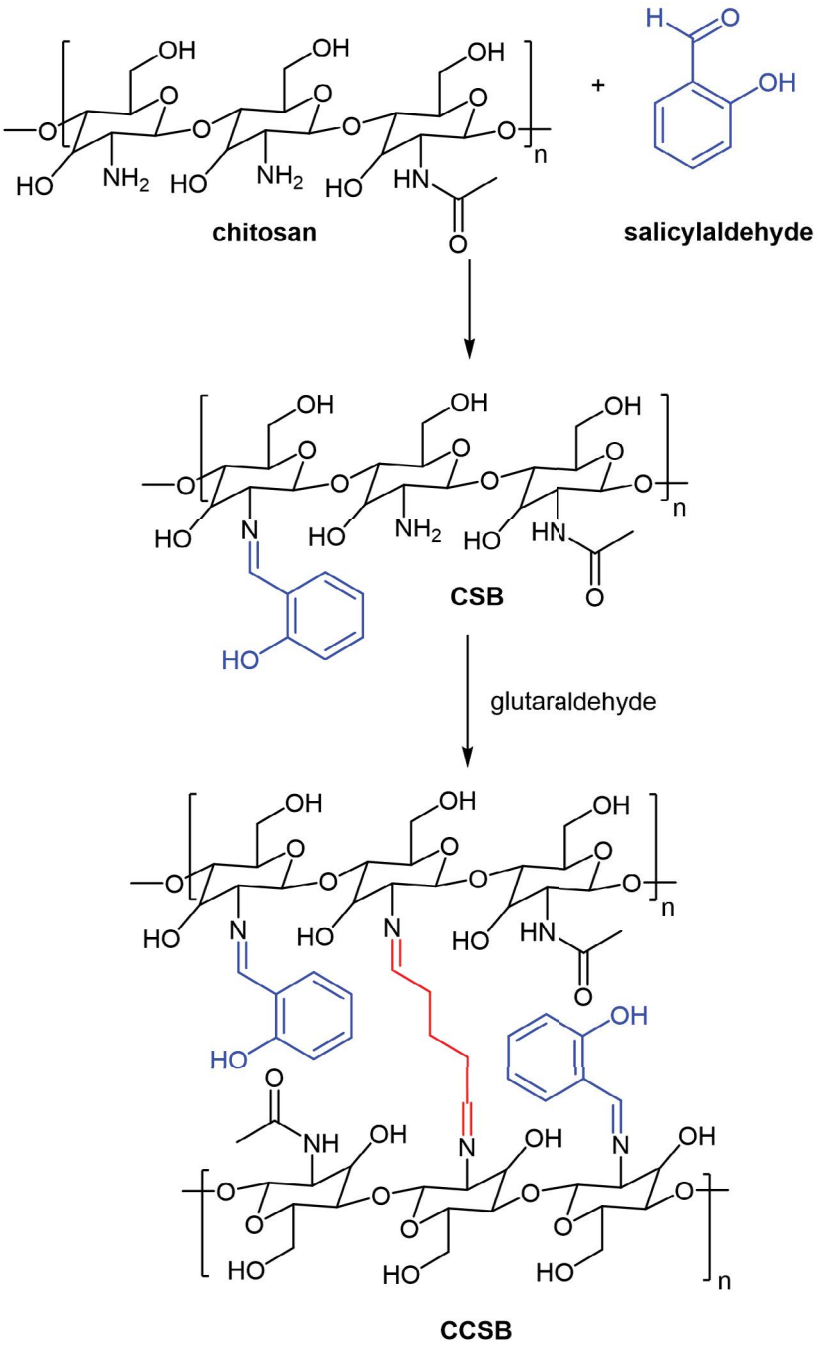


Fig. 1. Synthesis steps of CCSB.

### 3.2. SEM and EDS analysis

The morphology of the CCSB surface and its elemental composition were studied by using SEM and EDS techniques, Fig. 3 shows the SEM micrographs and EDS spectra of chitosan and CCSB. The surface of the chitosan appears relatively smooth while the surface of CCSB appears rough and irregular with small visible randomly distributed pockets indicating that the structural modification and the cross-linking affect the smoothness of the surface. The concentrations of the elements (C, O and N) as weight percentage (wt.%) for both chitosan and CCSB were estimated by using EDS analysis, the significant increment in the wt.% of C reflects the addition of carbon atoms to the chitosan after its condensation with salicylaldehyde and cross-linking with glutaraldehyde.

### 3.3. Effect of contact time on MO adsorption

Studying the relationship between the contact time and removal efficiency gives information about how the adsorption process occurs, the time profile tells how rapid is the adsorption process and how long is the time required

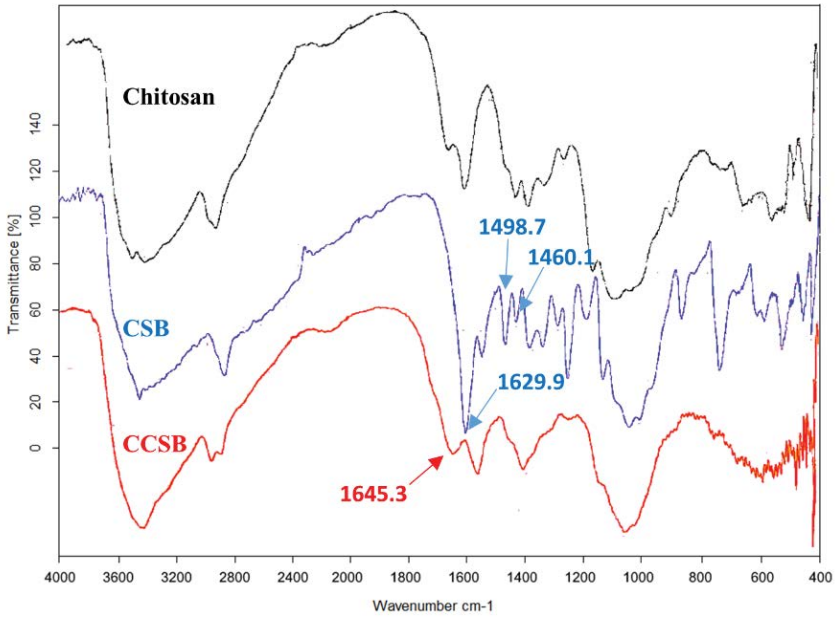


Fig. 2. FT-IR spectra of chitosan, CSB and CCSB.

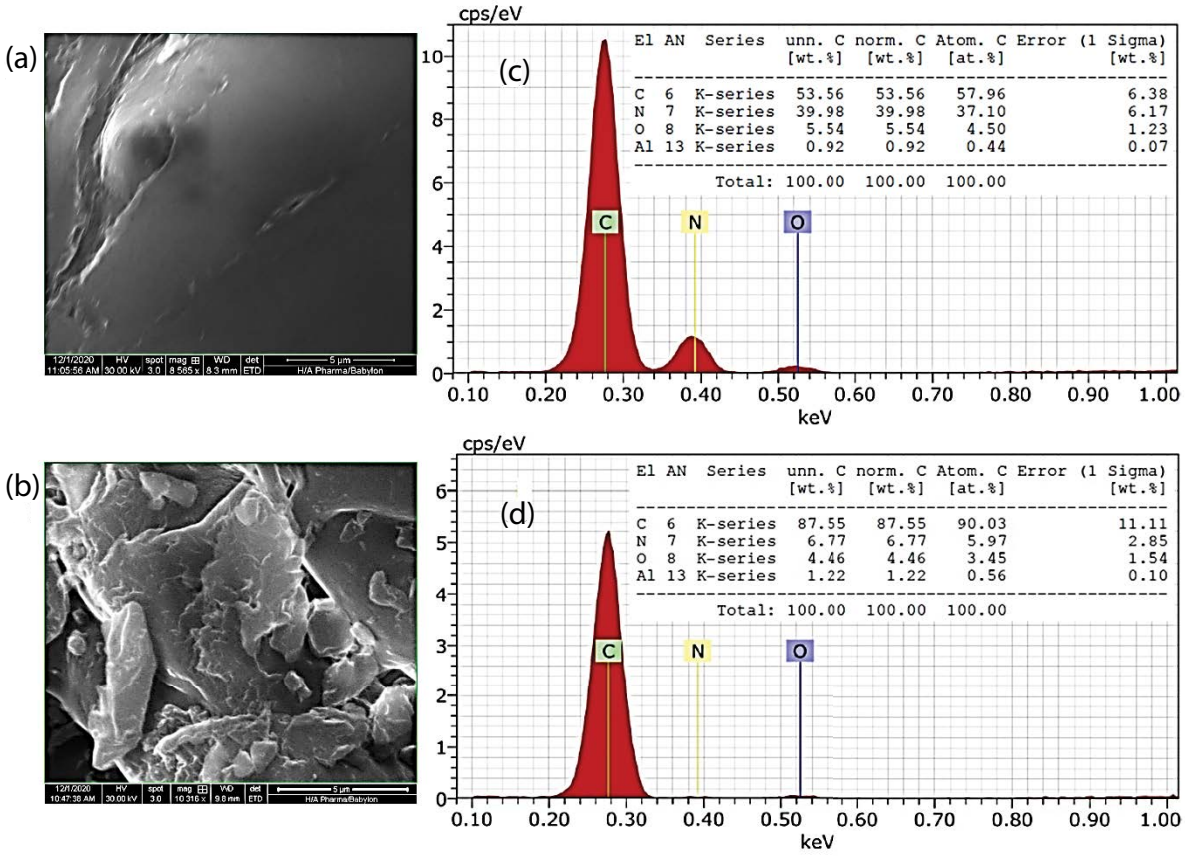


Fig. 3. SEM and EDS analysis for chitosan (a) and CCSB (b).

to reach the maximum removal efficiency, the point which indicates that the process has reached the equilibrium and no significant changes in the removal efficiency will be observed after that. Here, portions of a fixed weight of CCSB (0.1 g) were treated with two different concentrations of MO (50 mL, 100, and 150 ppm) the removal efficiency

was measured at different time intervals, Fig. 4 shows the obtained results. The adsorption of MO on CCSB takes 40 min to reach the equilibrium point.

### 3.4. Effect of pH of medium on MO adsorption

The pH of the MO aqueous solution is an important variable that influences the adsorption process and affects the removal efficiency. A fixed weight of CCSB was used to treat MO solutions with fixed concentration and different pH values (2–10). Fig. 5 illustrates the obtained results, the change of the pH values has no significant effect on the adsorption process, and very close removal efficiency values ($R$%) were recorded. This indicates that changing the pH does not make a significant change in the electrostatic properties of the CCSB surface and in this case, the mechanism of adsorption of MO on CCSB mainly depends on the π-π interactions between the phenyl rings of the modified polymer (CCSB) and those of methyl orange molecules.

### 3.5. Effect of initial MO concentration

The effect of the dye concentration was studied, different MO concentrations (200, 250, 300, 350, 400, 450, and 500 ppm) were treated with 0.10 g of the adsorbent. Slight gradual decrements in the removal percentage values accompanied by significant increments in the adsorption capacity values were observed with increasing the MO concentration, the minimum removal percentage (93.52%) and maximum removal capacity (233.8 mg/g) values were recorded for the highest concentration (500 ppm), Fig. 6. The inverse proportion between the initial dye concentration and the removal percentage is connected with the ratio of the numbers of the dye molecules at the initial concentrations to the adsorption centers on the adsorbents surface, at lower

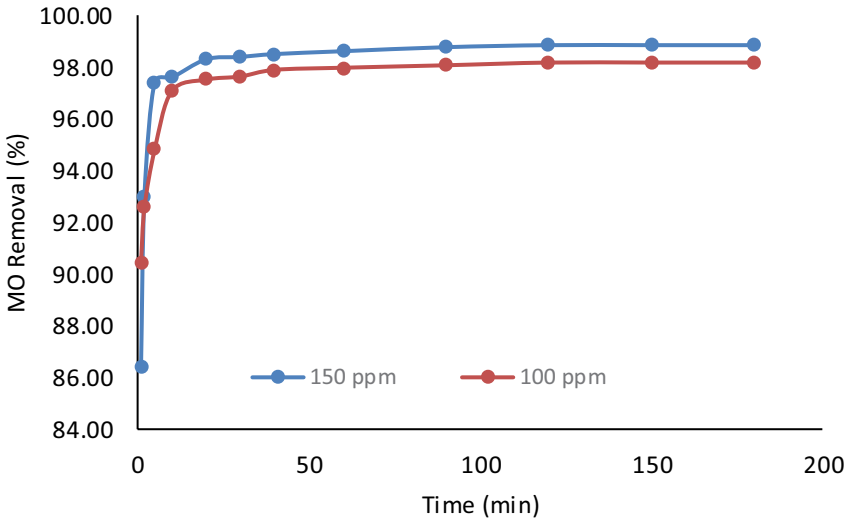


Fig. 4. Effect of contact time on adsorption of MO on CCSB.

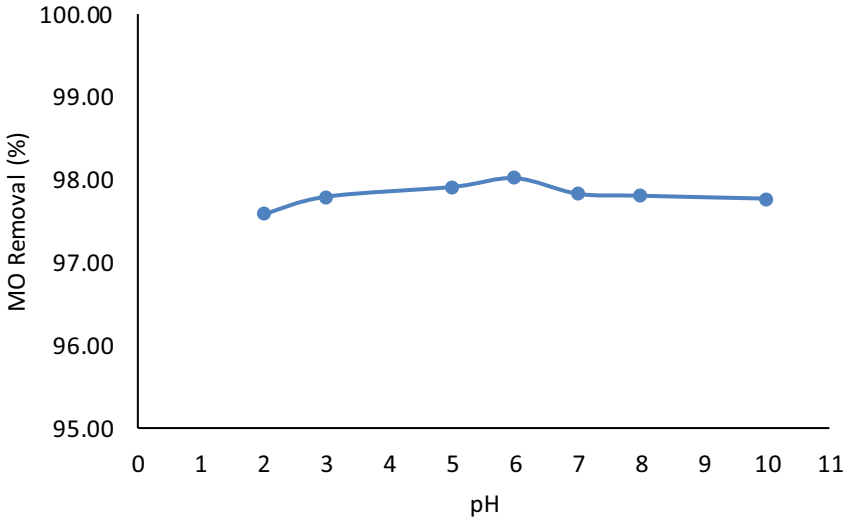


Fig. 5. Effect of pH on adsorption of MO on CCSB.

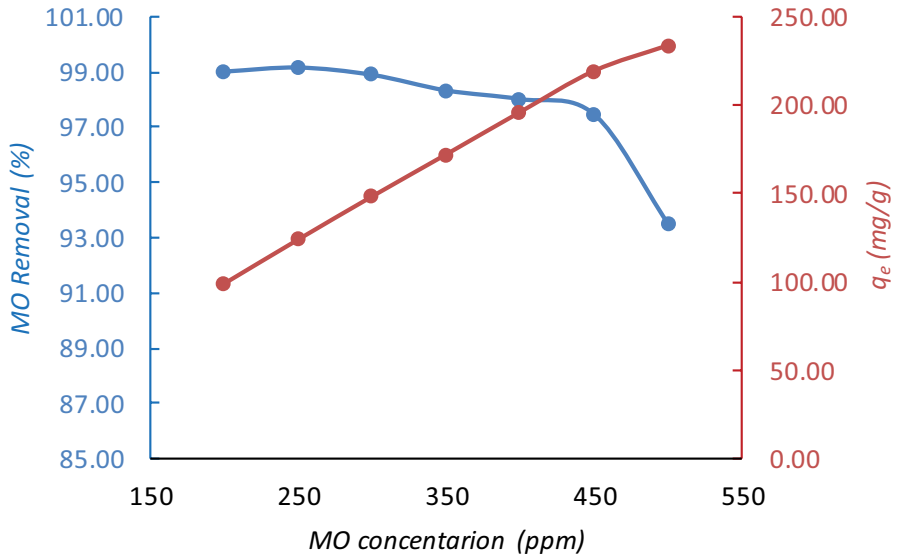


Fig. 6. Effect of initial concentration on adsorption of MO on CCSB.

initial dye concentrations the number of the free adsorption centers is relatively higher than in the case with higher dye concentration, so the removal percentage for the lower concentrations will be higher and vice versa.

### 3.6. Adsorption isotherms

To understand the nature of the adsorption of MO on CCSB, different isotherm models were implemented on the experimental equilibrium data. Langmuir [22], Freundlich [23], and Temkin [24] are represented in Figs. 7–9 respectively, the calculated data are reported in Table 1. The highest correlation coefficient ($R^2$) value was recorded for Langmuir isotherm (0.9984), this suggests that the adsorption of MO on CCSB obeys this isotherm.

According to Langmuir isotherm, it is assumed that the adsorbate molecules (MO in this case) form a monolayer on the homogeneous surface of the adsorbent (CCSB in this case). The linear form of Langmuir isotherm is expressed in Eq. (2):

$$\frac{C_e}{q_e} = \frac{C_e}{Q_0} + \frac{1}{Q_0 b} \tag{2}$$

where $C_e$ is the equilibrium solution concentration (mg/L), $q_e$ is the weight of the adsorbed dye per unit weight of adsorbent (mg/g); $Q_0$ is the maximum adsorption capacity, and $b$ is the Langmuir constants related to the rate of adsorption. Fig. 7 shows the Langmuir adsorption isotherm generated by plotting $C_e/q_e$ vs. $C_0$, the $Q_0$ and $b$ were calculated from the numerical slope and intercept values. In this study, the calculated $Q_0$ is 250 mg/g, and $b$ is 0.417 L/mg. Another characteristic constant that can be calculated for Langmuir adsorption model is the separation constant $R_L$, this dimensionless constant is also called the equilibrium constant that explain the degree of feasibility and favorability of the adsorption process, when ($R_L$ > 1) the adsorption is unfavorable; when ($R_L$ = 1) it is linear; when ($0 < R_L < 1$) it is favorable; when ($R_L$ = 0) it is irreversible [24]. The $R_L$ is expressed by Eq. (3):

$$R_L = \frac{1}{1 + bC_0} \tag{3}$$

where $b$ is the Langmuir constant (L/mg) and $C_0$ is the initial highest concentration of the dye (mg/L). Here, the separation factor was found to be 0.0053 indicating that the adsorption of MO on CCSB happens as a favorable process.

The obtained experimental data were also fitted to Freundlich isotherm which is expressed in Eq. (4):

$$\log q_e = \log K_f + \frac{1}{n}\log C_e \tag{4}$$

where $K_f$ and $n$ are the Freundlich constants, $K_f$ represents the adsorption capacity in mg/g and $n$ represents the adsorption intensity on the heterogeneous surface, this model suggests that the adsorption process is not limited to the formation monolayer on the adsorbent surface. By plotting $\log q_e$ vs. $\log C_e$ the Freundlich isotherm was obtained, Fig. 8, the $K$ and $n$ values were determined from the intercept slope respectively.

Temkin isotherm was also studied, this model assumes that the adsorbent–adsorbate interactions make the heat of adsorption of all of the adsorbate molecules in the formed layer decreases with coverage in a linear manner. The linear form of Temkin isotherm model is represented in Eq. (5):

$$q_e = B\ln K_t + B\ln C_e \tag{5}$$

where $B$ is constant which is associated with the heat of adsorption, and $K_t$ is Temkin isotherm constant (L/mg). This model was obtained by plotting $q_e$ vs. $\ln C_e$, Fig. 9, the values of the constants were determined from the values of slope and intercept.

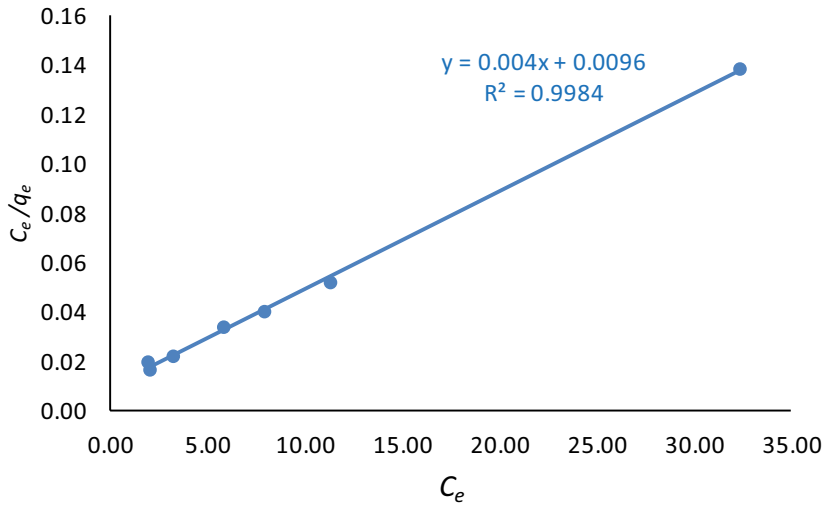


Fig. 7. Langmuir isotherm plot for adsorption of MO on CCSB.

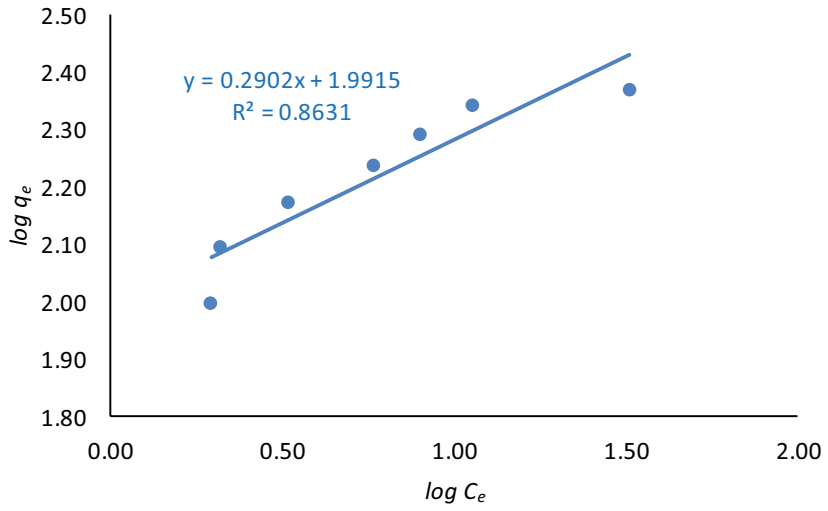


Fig. 8. Freundlich isotherm plot for adsorption of MO on CCSB.

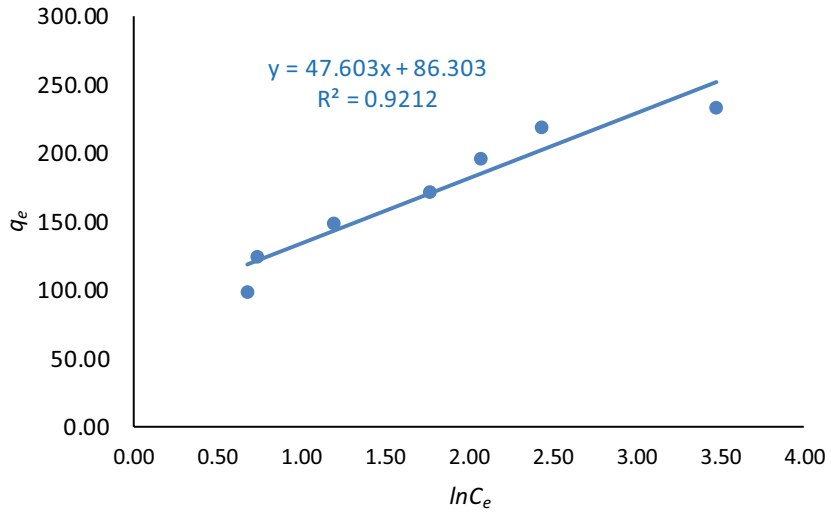


Fig. 9. Temkin isotherm plot for adsorption of MO on CCSB.

### 3.7. Adsorption kinetics

To get further details about the adsorption efficiency, the kinetics of the process have been studied. The amount of MO adsorbed on the CCSB at different time intervals was determined according to equation 6. The obtained experimental data were then applied on Lagergren pseudo-first-order and Ho pseudo-second-order models according to Eqs. (7) and (8) respectively [25,26].

$$q_t = \frac{(C_0 - C_t)V}{W} \tag{6}$$

$$\log(q_e - q_t) = \log q_e - \frac{k_1}{2.302}t \tag{7}$$

$$\frac{t}{q_t} = \frac{1}{k_2 q_e^2} + \frac{1}{q_e}t \tag{8}$$

where $q_e$ and $q_t$ is the amount of MO (mg/g) adsorbed on CCSB equilibrium and at time $t$ respectively, $V$ is the volume of the dye solution (L), $W$ is the mass of CCSB (g), $C_0$ is the initial MO concentration and $C_t$ is the concentrations of MO at time $t$, $k_1$ (min$^{-1}$) and $k_2$ (mg/g min) are the pseudo-first-order and pseudo-second-order rate constants. Fig. 10 shows the plot of $\log(q_e - q_t)$ vs. $t$ for the Lagergren pseudo-first-order model and Fig. 11 shows the plot of $t/q_t$ vs. $t$ for the Ho pseudo-second-order model. Table 2 involves correlation coefficients ($R^2$) the kinetic parameters calculated from the slope and intercept values for each model. The $R^2$ values for the pseudo-first-order model were found to be 0.8186 and 0.7836 for the 100 and 150 ppm concentrations respectively, in contrast for the pseudo-second-order model the $R^2$ values were exactly 1 for both concentrations. Furthermore, the theoretical values of $q_e$ that obtained from the pseudo-second-order model are very close to the experimental values ($q_{e,\exp}$) at the both tested initial dye concentrations. These results suggest that adsorption of MO on CCSB typically fits the pseudo-second-order model.

### 3.8. Adsorption thermodynamic parameters

The thermodynamic parameters for the adsorption process, free energy ($\Delta G$), enthalpy ($\Delta H$), and entropy ($\Delta S$) have been determined by Eqs. (9)–(11):

$$K_c = \frac{C_{Ae}}{C_e} \tag{9}$$

$$\ln K_c = -\frac{\Delta H}{RT} + \frac{\Delta S}{R} \tag{10}$$

$$\Delta G = \Delta H - T\Delta S \tag{11}$$

where $K_c$ is the equilibrium constant, $C_{Ae}$ is the weight of MO adsorbed on CCSB per liter of the solution at

Table 1
Parameters of the Langmuir, Freundlich and Temkin isotherm models

| Langmuir isotherm | | | | Freundlich isotherm | | | Temkin isotherm | | |
|---|---|---|---|---|---|---|---|---|---|
| $Q_0$ (mg/g) | $B$ (L/mg) | $R_L$ | $R^2$ | $K_f$ (mg/g)(L/mg)$^{1/n}$ | $n$ | $R^2$ | $K_t$ (L/mg) | $B$ | $R^2$ |
| 250.0 | 0.417 | 0.0053 | 0.9984 | 98.062 | 3.446 | 0.8631 | 6.129 | 47.603 | 0.9212 |

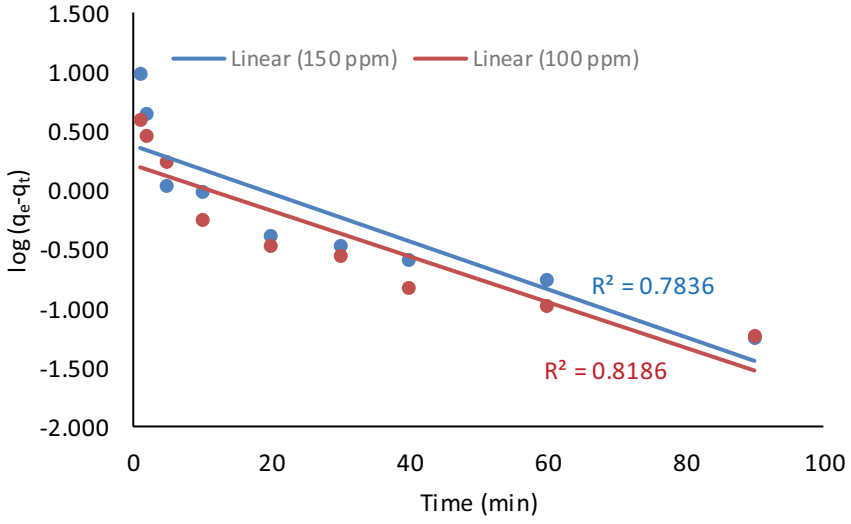


Fig. 10. Lagergren first-order kinetic plot for the sorption of MO on CCSB.

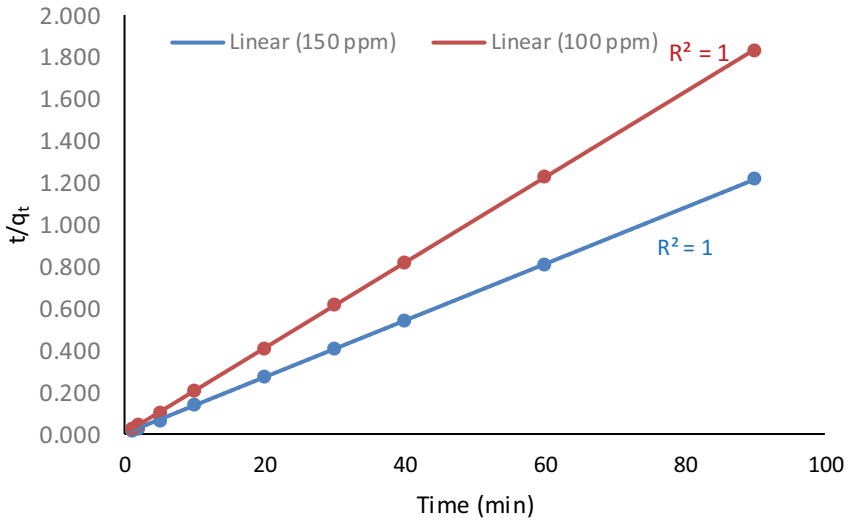


Fig. 11. Second-order kinetic plot for the sorption of MO on CCSB.

equilibrium (mg/L), $C_e$ is the equilibrium concentration of the dye in the solution (mg/L), $T$ is the absolute temperature (K), and $R$ is the universal gas constant (8.314 J/mol K).

Fig. 12 represents the plot of $\ln K_c$ vs. $1/T$, the $\Delta S$ and $\Delta H$ values were calculated from the slope and intercept of the generated linear curve according to Eq. (10), then the $\Delta G$ values were determined from the obtained results according to Eq. (11). Table 3 illustrate the calculated thermodynamic parameters, the negative $\Delta G$ values indicate that the adsorption of MO on CCSB happens spontaneously, and increasing these values with increasing the temperature shows that at a higher temperature the amount of MO adsorbed on CCSB increases. The positive $\Delta H$ value indicates that the process is endothermic and the positive $\Delta S$ value indicates increasing the disorder of molecules at the adsorbent-solution interface.

Table 2
Kinetic parameters for pseudo-first-order and pseudo-second-order

| | | Pseudo-first-order | | | Pseudo-second-order | | |
|---|---|---|---|---|---|---|---|
| $C_0$ (ppm) | $q_{e,exp}$ (mg/g) | $k_1$ (min$^{-1}$) | $q_e$ (mg/g) | $R^2$ | $k_2$ (mg/g min) | $q_e$ (mg/g) | $R^2$ |
| 100 | 49.09 | 0.044 | 1.62 | 0.8186 | 0.154 | 49.02 | 1 |
| 150 | 74.13 | 0.047 | 2.37 | 0.7836 | 0.107 | 74.07 | 1 |

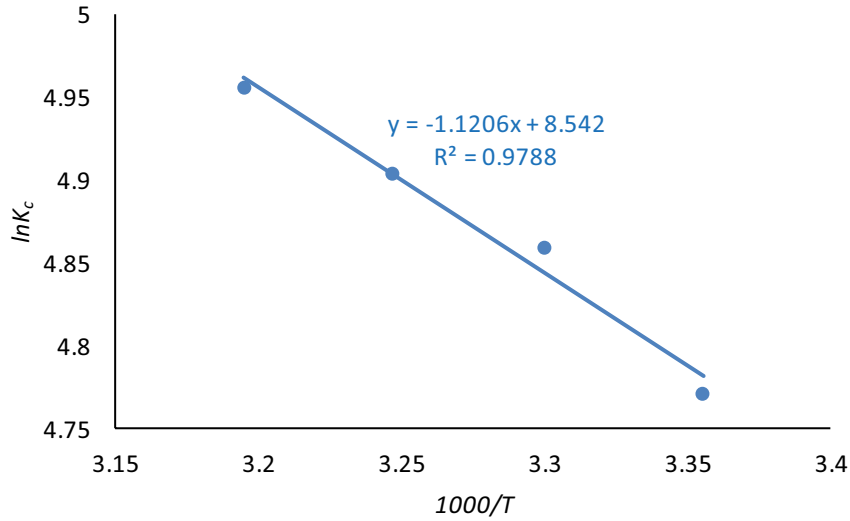


Fig. 12. Plot of $\ln K_c$ vs. $1/T$ for MO adsorption on CCSB.

### 3.9. Comparison of adsorption capacity of CCSB with other modified chitosan systems

In terms of adsorption capacity values, here we compare CCSB with other reported chitosan based adsorbents. Table 4 shows the values of the maximum adsorption capacity of CCSB for MO in comparison with other reported modified chitosan adsorbents for the same dye (MO). It is clear that CCSB has a much higher adsorption capacity (233.80 mg/g) when compared with the highest reported chitosan system, 98.30 mg/g for the protonated cross-linked chitosan. In other words, CCSB removes much higher MO quantities from aqueous solutions than the other compared adsorbents when treated with the same amount of them.

## 4. Conclusions

A CCSB was readily synthesized by the condensation between chitosan and salicylaldehyde followed by cross-linking with glutaraldehyde, it was characterized using FT-IR and SEM analysis. The synthesized polymer was used as an efficient adsorbent for the removal of MO from aqueous solution with high removal percentage over pH range 2–10. The adsorption capacity of CCSB for methyl orange be 233.8 mg/g which was much higher than other reported adsorbents with a similar structural backbone (chitosan). The adsorption data followed Langmuir isotherm model and the kinetic studies indicated that the adsorption process is pseudo-second-order. The thermodynamic studies showed a spontaneous, endothermic adsorption process.

Table 3
Thermodynamic parameters for adsorption of MO on CCSB

| Temperature | $\Delta G$ (kJ/mol) | $\Delta H$ (kJ/mol) | $\Delta S$ (J/mol/K) |
|---|---|---|---|
| 298 | –11.846 | 9.317 | 71.018 |
| 303 | –12.201 | | |
| 308 | –12.557 | | |
| 313 | –12.912 | | |

Table 4
Adsorption capacities ($Q_0$) of MO on different analogues adsorbents

| Adsorbent | $Q_0$ (mg/g) | Reference |
|---|---|---|
| Chitosan biomass | 29.00 | [27] |
| Chitosan 10B | 8.41 | [28] |
| Chitosan/alumina composite | 29.99 | [29] |
| Magnetic/maghemite chitosan films | 28.94 | [30] |
| Magnetic chitosan enwrapped with MWCNTs | 60.50 | [31] |
| Heterocyclic chitosan-based Schiff base | 55.55 | [19] |
| Protonated cross-linked chitosan | 89.30 | [1] |
| CCSB | 233.80 | This study |

## Acknowledgment

The authors would like to thank the University of Babylon and the University of Karbala for the financial support.

## References

[1] R. Huang, Q. Liu, J. Huo, B. Yang, Adsorption of methyl orange onto protonated cross-linked chitosan, Arabian J. Chem., 10 (2017) 24–32.
[2] S. Chen, J. Zhang, C. Zhang, Q. Yue, Y. Li, C. Li. Equilibrium and kinetic studies of methyl orange and methyl violet adsorption on activated carbon derived from *Phragmites australis*, Desalination, 252 (2010) 149–156.
[3] B. Lellis, C.Z. Fávaro-Polonio, J.A. Pamphile, J.C. Polonio, Effects of textile dyes on health and the environment and bioremediation potential of living organisms, Biotechnol. Res. Innovation, 3 (2019) 275–290.
[4] G. Sheng, L. Ye, Y. Li, H. Dong, H. Li, X. Gao, Y. Huang, EXAFS study of the interfacial interaction of nickel(II) on titanate nanotubes: role of contact time, pH and humic substances, Chem. Eng. J., 248 (2014) 71–78.
[5] K. Rajeshwar, M.E. Osugi, W. Chanmanee, C.R. Chenthamarakshan, M.V.B. Zanoni, P. Kajitvichyanukul, R. Krishnan-Ayer, Heterogeneous photocatalytic treatment of organic dyes in air and aqueous media, J. Photochem. Photobiol., C, 9 (2008) 171–192.
[6] S. Kiran, S. Ali, M. Asgher, Degradation and mineralization of azo dye reactive blue 222 by sequential photo-Fenton's oxidation followed by aerobic biological treatment using white rot fungi, Bull. Environ. Contam. Toxicol., 90 (2013) 208–215.
[7] S.C.R. Santos, R.A.R. Boaventura, Adsorption of cationic and anionic azo dyes on sepiolite clay: equilibrium and kinetic studies in batch mode, J. Environ. Chem. Eng., 4 (2016) 1473–1483.
[8] S. Wong, Y. Lim, N. Ngadi, R. Mat, O. Hassan, I.M. Inuwa, N.B. Mohamed, J.H. Low, Removal of acetaminophen by activated carbon synthesized from spent tea leaves: equilibrium, kinetics and thermodynamics studies, Powder Technol., 338 (2018) 878–886.
[9] G. Bayramoglu, G. Kunduzcu, M.Y. Arica, Preparation and characterization of strong cation exchange terpolymer resin as effective adsorbent for removal of disperse dyes, Polym. Eng. Sci., 60 (2020) 192–201.
[10] M. Groß, M.T. Lima, M. Uhlig, A. Ebraheme, O. Roeber, B. Olschewski, R. von Klitzing, R. Schomäcker, M. Schwarze, Biopolymers for dye removal via foam separation, Sep. Purif. Technol., 188 (2017) 451–457.
[11] S. Wong, N. Abd Ghafar, N. Ngadi, F.A. Razmi, I.M. Inuwa, R. Mat, N.A.S. Amin, Effective removal of anionic textile dyes using adsorbent synthesized from coffee waste, Sci. Rep., 10 (2020) 1–13.
[12] L. Deng, H. Zeng, Z. Shi, W. Zhang, J. Luo, Sodium dodecyl sulfate intercalated and acrylamide anchored layered double hydroxides: a multifunctional adsorbent for highly efficient removal of Congo red, J. Colloid Interface Sci., 521 (2018) 172–182.
[13] D. Sasmal, J. Maity, H. Kolya, T. Tripathy, Study of congo red dye removal from its aqueous solution using sulfated acrylamide and N, N-dimethyl acrylamide grafted amylopectin, J. Water Process Eng., 18 (2017) 7–19.
[14] J. Ray, S. Jana, T. Tripathy, Synthesis of dipolar grafted hydroxyethyl cellulose and its application for the removal of phosphate ion from aqueous medium by adsorption, Int. J. Biol. Macromol., 109 (2018) 492–506.
[15] R. Laus, V.T. De Favere, Competitive adsorption of Cu(II) and Cd(II) ions by chitosan crosslinked with epichlorohydrin–triphosphate, Bioresour. Technol., 102 (2011) 8769–8776.
[16] B.F. Senkal, E. Yavuz, Preparation of poly(vinyl pyrrolidone) grafted sulfonamide based polystyrene resin and its use for

the removal of dye from water, Polym. Adv. Technol., 17 (2003) 928–931.
[17] P.D. Chethan, B. Vishalakshi, Adsorption efficiency of Cr(VI) by ethylene-1,2-diamine-6-deoxychitosan, Sep. Sci. Technol., 50 (2015) 1158–1165.
[18] Z.A. Sutirman, M.M. Sanagi, K.J. Abd Karim, W.A.W. Ibrahim, Preparation of methacrylamide-functionalized crosslinked chitosan by free radical polymerization for the removal of lead ions, Carbohydr. Polym., 151 (2016) 1091–1099.
[19] A.S. Manchaiah, V. Badalamoole, Novel heterocyclic chitosan-based Schiff base: evaluation as adsorbent for removal of methyl orange from aqueous solution, Water Environ. J., 34 (2020) 364–373.
[20] R. Menaka, S. Subhashini, Chitosan Schiff base as eco-friendly inhibitor for mild steel corrosion in 1 M HCl, J. Adhes. Sci. Technol., 30 (3016) 1622–1640.
[21] P. Zhao, M. Xin, M. Li, J. Deng, Adsorption of methyl orange from aqueous solution using chitosan microspheres modified by β-cyclodextrin, Desal. Water Treat., 57 (2016) 11850–11858.
[22] I. Langmuir, The adsorption of gases on plane surfaces of glass, mica and platinum, J. Am. Chem. Soc., 40 (1918) 1361–1403.
[23] H.M.F. Freundlich, Over the adsorption in solution, J. Phys. Chem., 57 (1906) 385–471.
[24] M.I. Temkin, Kinetics of ammonia synthesis on promoted iron catalysts, Acta Physicochimica URSS, 12 (1940) 327–356.
[25] S. Lagergren, Zur theorie der sogenannten adsorption geloster stoffe, Kungliga Svenska Vetenskapsakademiens. Handlingar, 24 (1898) 1–39.
[26] Y.S. Ho, G. McKay, The kinetics of sorption of divalent metal ions onto sphagnum moss peat, Water Res., 34 (2000) 735–742.
[27] F.-N. Allouche, N. Yassaa, H. Lounici, Sorption of methyl orange from aqueous solution on chitosan biomass, Procedia Earth Planet Sci., 15 (2015) 596–601.
[28] T.K. Saha, N.C. Bhoumik, S. Karmaker, M.G. Ahmed, H. Ichikawa, Y. Fukumori, Adsorption of methyl orange onto chitosan from aqueous solution, J. Water Resour. Prot., 2 (2010) 898–906.
[29] J. Zhang, Q. Zhou, L. Ou, Kinetic, isotherm, and thermodynamic studies of the adsorption of methyl orange from aqueous solution by chitosan/alumina composite, J. Chem. Eng. Data, 57 (2012) 412–419.
[30] R. Jiang, Y.Q. Fu, H.Y. Zhu, J. Yao, L. Xiao, Removal of methyl orange from aqueous solutions by magnetic maghemite/chitosan nanocomposite films: adsorption kinetics and equilibrium, J. Appl. Polym. Sci., 125 (2012) E540–E549.
[31] H.Y. Zhu, R. Jiang, L. Xiao, G.M. Zeng, Preparation, characterization, adsorption kinetics and thermodynamics of novel magnetic chitosan enwrapping nanosized γ-$Fe_2O_3$ and multi-walled carbon nanotubes with enhanced adsorption properties for methyl orange, Bioresour. Technol., 101 (2010) 5063–5069.